Optimizing the Quench Protection of a 13 T Nb_3Sn Common-Coil Magnet

E. Ravaioli, D. Araujo, B. Auchmann, A. Verweij, and M. Wozniak

***Abstract*—A 13 T Nb_3Sn common-coil accelerator-type magnet is being developed at the Paul Scherrer Institute (PSI). The magnet cross-section features an innovative design with asymmetric elements and effective stress-management. Thanks to the asymmetric design narrow pole racetrack coils are not required in proximity of the magnet apertures to improve the field quality. Its magnetic design achieves adequate margin with respect to the short-sample limit while utilizing two available cables. This choice accelerates the completion of the 0.8 m long demonstrator magnet, but limits the flexibility of the conductor grading and makes the magnet quench protection more challenging. In this contribution, the strategy to limit the hot-spot temperature and peak voltage to ground reached in the magnet conductor after a quench is discussed. The electromagnetic and thermal transients occurring during a quench discharge are simulated with the STEAM-LEDET program. Quench detection based on differential-voltage monitoring is proposed, and the expected quench detection times are evaluated in the case of quenches occurring in different coil locations. Furthermore, the performances of various quench protection systems, including energy-extraction based either on a resistor or a varistor, a CLIQ (Coupling-Loss Induced Quench) system, or combinations of these are assessed. It is shown that while energy-extraction is a viable option to protect the magnet, acceptable performance can be achieved with CLIQ while achieving a significantly lower peak voltage to ground. The lowest hot-spot temperature is obtained by combining energy extraction and CLIQ.**

***Index Terms*—Accelerator magnet, CLIQ, magnet design, quench protection, simulation, superconducting coil.**

I. Introduction

An innovative concept for common-coil magnets was recently proposed, which features stress-management of turn blocks and an asymmetric disposition of the turns around the aperture [1]. A very attractive property of this design is that it only relies on common-coils also for the pole turns, contrarily to previous common-coil designs. Hence, its construction is simplified and all of its turns have large bending radius.

In order to demonstrate this Stress-Managed Asymmetric Common-Coil (SMACC) technology, a subscale stress-managed symmetric magnet was successfully built at PSI and tested at the CERN magnet test facility [2]. Furthermore, a 13 T, 4 layers, Nb_3Sn magnet, whose main parameters are summarized in Table I, is developed at the Paul Scherrer Institute (PSI).

TABLE I
Main Magnet Parameters [1]

Parameter	Unit	Value
Bore magnetic field	T	13.0
Intra-beam distance	mm	250
Bore diameter	mm	50
Magnetic length	m	0.8
Operating temperature, T_{op}	K	4.2
Operating current, I_{op}	A	14050
Margin at T_{op}, i.e. $I_{\mathrm{op}}/I_{\mathrm{ss}}$	-	9.5%
Self-inductance at I_{op}	mH/m	22.3
Stored energy at I_{op}	MJ/m	2.2
Number of turns per pole	-	150

The magnet coils are surrounded by an iron yoke with an outer radius of 720 mm. Although this magnet has a relatively short magnetic length of 0.8 m, its quench protection is challenging. In fact, its design is optimized for magnetic performance and appropriate stress-management, and not for the quench protection performance. Furthermore, the constraint of utilizing two available cables with quite different cross-sections eliminates any flexibility in the conductor grading. The protection of a longer SMACC magnet, which will require updating the cross-section and the conductor grading, will be examined in future works.

Different options are explored as an active quench protection system, including energy-extraction (EE) based on a resistor (EER) or a varistor (EEV), Coupling-Loss Induced Quench (CLIQ) method [3], [4], and combinations of these. The quench protection is designed to maintain the coil's hot-spot temperature below 350 K, which is considered a safe limit with respect to permanent degradation, and the peak voltage to ground below 1 kV. A few limitations are imposed by the test station where the magnet will be tested. The peak voltage across the energy-extraction unit U_{EE} [V] must remain below 1 kV, and the peak voltage across the CLIQ unit U_{c} [V] and the current through it I_{C} [A] must remain below 1 kV and 5 kA, respectively.

The common-coil geometry allows for flexibility in the selection of the CLIQ configuration. In fact, it is possible to include CLIQ current leads between individual layers, which gives multiple connection options resulting in very different performances. The combinations of EE voltage ratings, CLIQ configurations, and CLIQ unit charging voltages that satisfy all requirements are sought by performing a comprehensive parametric analysis using the STEAM-LEDET software [5], [6].

Received 21 September 2024; revised 10 December 2024; accepted 14 December 2024. Date of publication 18 December 2024; date of current version 17 January 2025. *(Corresponding author: E. Ravaioli.)*

E. Ravaioli, A. Verweij, and M. Wozniak are with CERN, CH-1211 Geneva, Switzerland (e-mail: Emmanuele.Ravaioli@cern.ch).

D. Araujo and B. Auchmann are with PSI, 5232 Villigen, Switzerland.

Color versions of one or more figures in this article are available at https://doi.org/10.1109/TASC.2024.3520067.

Digital Object Identifier 10.1109/TASC.2024.3520067

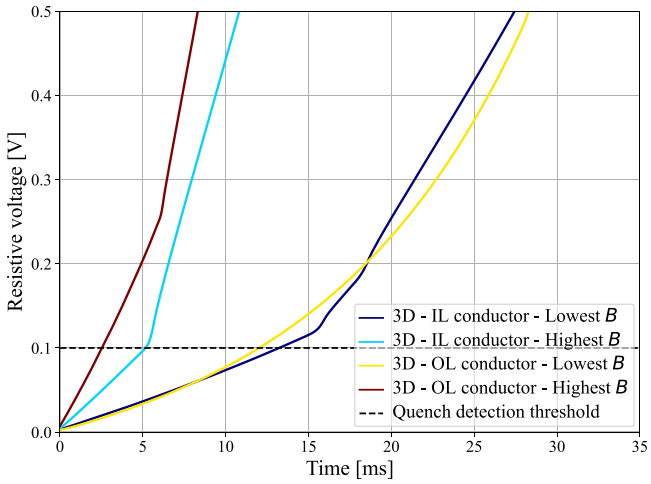

Fig. 1. Simulation of quench development in the common-coil magnet at nominal current. Coil resistive voltage versus time, for four initial quench locations with different conductors and magnetic field (see Table II).

TABLE II
MAIN PARAMETERS OF INNER AND OUTER LAYERS CONDUCTORS [1]

Parameter	Unit	Inner	Outer
Superconductor/Stabilizer	-	Nb_3Sn/Cu	Nb_3Sn/Cu
Critical current at 16 T, 4.2 K	A	618	206
Number of strands	-	21	34
Strand diameter	mm	1.1	0.7
Cu/noCu ratio	-	0.9	1.2
Bare cable width	mm	12.74	12.77
Bare cable height	mm	2.06	1.30
Insulation thickness	mm	0.15	0.15
Current density in stabilizer	A/mm^2	1486	1969
$\xi = J^2/f_{\rm ST}$	A^2/mm^4	1046	2114
Highest magnetic field at $I_{\rm op}$	T	14.2	11.2

II. QUENCH DETECTION

The proposed quench detection strategy is based on monitoring the differential voltage between magnet coil sections. When the voltage difference is higher than a threshold $U_{\rm qd}$ [V] for a time longer than the discrimination time $t_{\rm d}$ [s], the power supply is switched off and the quench protection system is activated. Based on previous experience with magnets made of similar conductors, a quench detection threshold of 100 mV and a discrimination time of 5 ms are good values to compromise between achieving fast detection and avoiding frequent spurious triggers.

The resistive voltage build-up after a quench is calculated using the STEAM-LEDET program, which includes three-dimensional thermal diffusion in the coil windings [7] and was extensively validated [8], [9], [10], [11], [12], [13]. The coil resistive voltages obtained for four quench locations with different conductors and magnetic fields B [T] are shown in Fig. 1. As expected, the voltage rise is strongly influenced by the magnetic field at the quench location, which impacts both the energy margin to quench and the local ohmic loss due to magneto-resistance [14]. Furthermore, the resistive voltage build-up differs in the conductors used in the two inner layers (IL) and in the two outer layers (OL), since they have different stabilizer cross-sections (see Table II).

The normal zone propagates to the turns in thermal contact with the initially quenched turn due to thermal diffusion across insulation layers. This is the cause of the slope change of the resistive voltage.

III. QUENCH PROTECTION

Active quench protection systems are designed to prevent coil damage caused by overheating of the hot-spot where the quench started by extracting part of the magnet stored energy or by actively heating the superconductor and transferring part of it to the normal state, hence distributing the magnet energy more uniformly in the coil windings [4], [15], [16], [17], [18].

The current density in the normal-conducting part of the conductor is often used as a quality factor to estimate quench protection performance. A more appropriate metric, which takes into account the actual physics involved in the hot-spot heating, is $\xi = J^2/f_{\rm ST}$ [A^2/m^4], with J [A/m^2] the conductor current density and $f_{\rm ST}$ the stabilizer fraction in the conductor [18]. In fact, let us consider a small length Δl [m] of a conductor with cross-section A [m^2]. The local heat balance equation applied to its volume $A\Delta l$ neglecting cooling is simply

$$\rho \frac{\Delta l}{f_{\rm ST} A} I^2 = \overline{c_{\rm v}} A \Delta l \frac{dT}{dt}, [W] \tag{1}$$

where ρ [Ωm] is the stabilizer electrical resistivity and $\overline{c_{\rm v}}$ [J/K/m^3] is the conductor volumetric heat capacity, weighted by the fractions of materials in its cross-section. It follows that the rate of change of the hot-spot temperature is

$$\frac{dT}{dt} = \frac{\rho}{\overline{c_{\rm v}}} \frac{J^2}{f_{\rm ST}} = \frac{\rho}{\overline{c_{\rm v}}} \xi, [K/s] \tag{2}$$

where the defined quantity ξ appears.

The ξ of the conductor used in the magnet outer layers is twice higher than the one in the inner layers. Since the peak field in these conductors is similar (see Table II), the temperature increase is approximately twice faster if the hot-spot occurs in the OL conductor. Thus, the worst case is a quench occurring in the highest-field turn of the OL conductor. In the case of a quench in this location the estimated quench detection time, i.e. the time at which the coil resistive voltage is higher than $U_{\rm qd}$, is about 2.5 ms, as can be seen in Fig. 1.

The total reaction time $t_{\rm R}$ [s] is the sum of three components: the quench detection time, the discrimination time, and the protection unit triggering time. The EE system available at the test facility features a mechanical switch with a characteristic triggering time of about 3.2 ms, while the CLIQ unit relies on thyristors that are triggered in about 0.1 ms [19]. Thus, the reference $t_{\rm R}$ are rounded up to be 11 ms and 8 ms for the EE and CLIQ systems, respectively.

A. Magnet Powering and Protection Circuit

The simplified electrical scheme of the magnet circuit is shown in Fig. 2, where the protection systems analyzed in this study are included: the energy-extraction system, including either a resistor ($R_{\rm EER}$) or a varistor ($R_{\rm EEV}$), and the CLIQ unit connected to the magnet coils through two leads. The

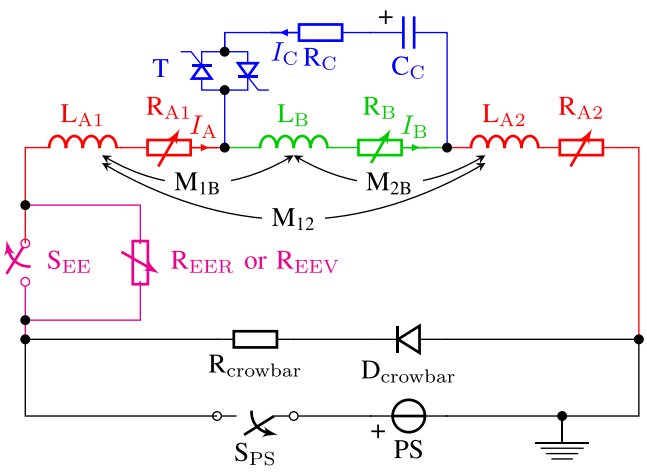

Fig. 2. Simplified electrical scheme of the magnet powering and protection circuit. The following elements are identified: power supply (PS), its switch (S_{PS}) that is opened to start the discharge, and its crowbar composed of a diode ($D_{crowbar}$) and a resistor ($R_{crowbar}$); magnet coil sections L_{A1}, L_{A2}, and L_B and their resistances R_{A1}, R_{A2}, and R_B; CLIQ unit connected across L_B, including a capacitor C_C, parasitic resistance R_C, and back-to-back thryristors T; energy extraction system composed of a switch (S_{EE}) and either a resistor (R_{EER}) or a varistor (R_{EEV}).

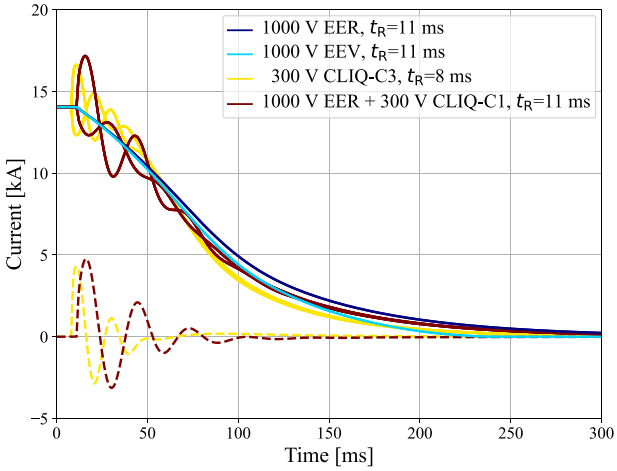

Fig. 3. Simulated current versus time after a quench at nominal current, for four analyzed quench protection configurations. For cases including CLIQ, the current I_C introduced by the CLIQ unit is also shown (dashed lines).

effectiveness of various protection options is assessed by simulating quench transients and evaluating the hot-spot temperature T_{hot} [K] and peak voltage to ground $U_{g,m}$ [V] in the coil windings, while respecting the constraint on the peak CLIQ current.

B. Energy Extraction

The simulated magnet current I_A [A] after a quench occurring at $t = 0$ in the highest-field turn of the OL conductor at the nominal current $I_{op} = 14050$ A is shown in Fig. 3 for four quench protection options. In the case of an EE system including a resistor, the current discharge is significantly faster than a simple exponential decay due the occurrence of coupling

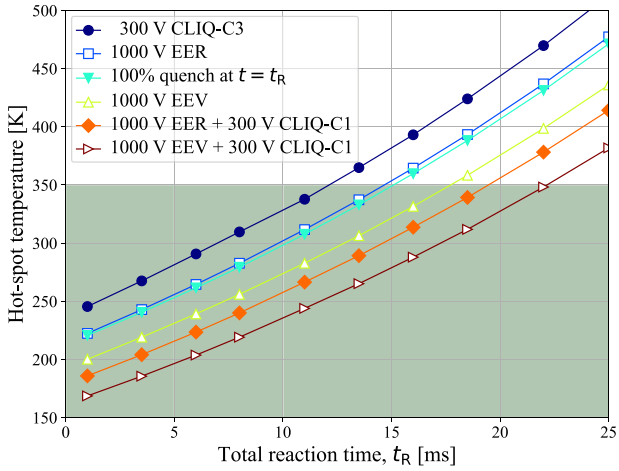

Fig. 4. Calculated adiabatic hot-spot temperature as a function of the total reaction time, for four analyzed quench protection configurations, after a quench occurring in the highest-field turn of the OL conductor. The same quantity is plotted in the case of an ideal quench protection system turning 100% of the magnet conductor to the normal state at $t = t_R$.

currents, which reduce the magnet differential inductance and cause quench-back, hence increasing the coil resistance [8].

The peak voltage in the coil windings coincides with the voltage across the EE, i.e. $R_{EE}I_{op} = 1$ kV for $R_{EE} = 71$ mΩ. Grounding the middle point of the EE resistor would allow effectively halving this value, but it is not feasible due to magnet test facility's constraints.

If a varistor is used in the EE rather than a linear resistor, the magnet energy can be discharged more quickly for the same peak voltage, as can be seen in Fig. 3. The varistor's equivalent resistance is approximated here as $R_{EEV}=R_0|I_A|^\gamma$, with $R_0 = 34.35\ \Omega A^{-\gamma}$ and $\gamma = -0.647$, which yields 71 mΩ for $I_A = I_{op}$. In this application, the quench load, i.e. the time integral of I_A^2, which is roughly proportional to the energy deposited in the hot-spot during the discharge, is reduced only by 6% when using the varistor rather than the constant resistor. This limited effect can be explained by the fact that in both cases the magnet coil resistance increases rapidly after the EE triggering due to quench-back, and at the end of the discharge it is about three times higher than R_{EE}.

The hot-spot temperature is calculated under adiabatic assumptions for both cases as a function of the total reaction time, and plotted in Fig. 4.

The use of a varistor can reduce T_{hot} by 20 to 40 K in the considered range of t_R. The EER and EEV systems can maintain T_{hot} below 350 K, which is considered a safe limit with respect to permanent degradation, for $t_R < 14$ ms and $t_R < 18$ ms, respectively.

C. Coupling-Loss Induced Quench System

An alternative quench protection option based on CLIQ is considered, which is characterized by a fast and effective heating mechanism based on transient losses [20], [21], [22]. The CLIQ unit available in the test station includes a 50 mF capacitor bank

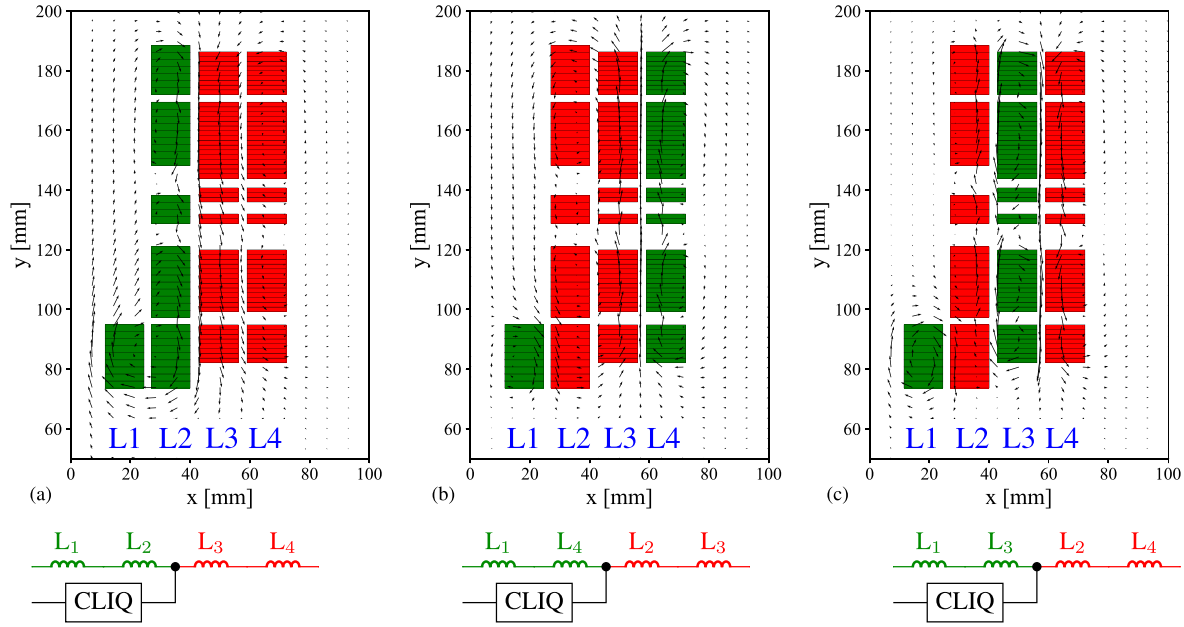

Fig. 5. Top plots: Polarities of CLIQ-induced current changes dI/dt in the coil windings (conductor filled colors) and resulting magnetic-field change (arrows), for the three CLIQ configurations (only half of a pole is shown). Bottom diagrams: Simplified electrical order and CLIQ connection scheme (only one of the two common-coils is shown). (a) CLIQ-C1: Same dI/dt in layers L1-L2 and L3-L4. (b) CLIQ-C2: Same dI/dt in layers L1-L4 and L2-L3. (c) CLIQ-C3: Same dI/dt in layers L1-L3 and L2-L4.

that can be charged up to 1 kV. The unit is connected to two terminals internal to the magnet coils (see Fig. 2). Upon triggering, fast current changes are introduced in the coil sections, which in turn generate high magnetic-field change rate dB/dt [T/s] and hence transient losses in the superconductor.

The positioning of the CLIQ connections and the coil electrical order are crucial for CLIQ performance. In the case of a magnet made of two common-coils, each composed of two double-pancakes (L1-L2 and L3-L4), three possible CLIQ configurations are identified, which are shown in Fig. 5. Configuration CLIQ-C1 is the easiest to implement, as it does not require CLIQ leads between coils of the same double-pancake.

Configurations that impose opposite current changes dI/dt [A/s] in physically-adjacent coil sections are more effective, because the equivalent inductance of the CLIQ discharge circuit is reduced, hence introducing higher dI/dt for the same CLIQ charging voltage U_{C0} [V], and because high transient losses are generated in the strands located at the interface between coil sections, where the dB/dt generated by the coil sections superpose [4], [23]. Observing Fig. 5, CLIQ-C3 is expected to be the best-performing configuration since it imposes opposite dI/dt in each consecutive layer.

The simulated currents in the magnet coil sections and introduced by the CLIQ unit I_{C} [A] in the case of a quench at I_{nom} protected by a 300 V CLIQ-C3 system are shown in Fig. 3. Although no energy is extracted by the protection system, the CLIQ-introduced transient losses extend the normal zone so quickly that the magnet's stored energy is dissipated rather uniformly in the coil windings. As a result, T_{hot} remains at 310 K for $t_{\mathrm{R}} = 8$ ms, as can be seen in Fig. 4.

TABLE III
MAIN QUENCH PROTECTION RESULTS AT NOMINAL CURRENT

Protection system	t_{R} [ms]	T_{hot} [K]	$U_{\mathrm{g,m}}$ [V]	$I_{\mathrm{C,m}}$ [kA]
1000 V EER	11	312	1000	-
1000 V EEV	11	283	1000	-
500 V CLIQ-C1	8	321	250	4.5
400 V CLIQ-C2	8	305	199	4.4
300 V CLIQ-C3	8	310	184	4.3
1000 V EER +300 V CLIQ-C1	11	266	1000	4.8
900 V EER +100 V CLIQ-C2	11	268	958	4.7
700 V EER +100 V CLIQ-C3	11	285	711	4.9
1000 V EEV +300 V CLIQ-C1	11	244	1000	4.9
900 V EEV +100 V CLIQ-C2	11	254	958	4.9
600 V EEV +100 V CLIQ-C3	11	283	605	4.7
Ideal 100% quench	8	279	396	-

The performances of the three different CLIQ systems adopting the three above-mentioned configurations are summarized in Table III, and compared to those of the EER and EEV systems.

For each configuration, the charging voltage of the CLIQ unit is optimized to reduce T_{hot} and $U_{\mathrm{g,m}}$ while respecting the constraint on the peak CLIQ current, $I_{\mathrm{C,m}} \leq 5$ kA. Note that if $t_{\mathrm{R}}=11$ ms was assumed for the CLIQ cases the corresponding T_{hot} would increase by about 30 K.

The best CLIQ configuration yields a T_{hot} only 26 K higher than that of an ideal system that instantaneously transfers the entire magnet conductor to the normal state at $t_{\mathrm{R}}=8$ ms (see Fig. 4 and Table III).

In the case of an energy-extraction system the peak voltage to ground is dominated by the voltage across the EE unit and coincides with $R_{\mathrm{EE}}I_{\mathrm{op}}$, while in the case of a CLIQ system it is dominated by the CLIQ unit voltage and is $U_{\mathrm{C,0}}/2$. Thus, for this magnet CLIQ can maintain the T_{hot} to levels similar to the EER and EEV systems, but with 4 to 5 times lower $U_{\mathrm{g,m}}$.

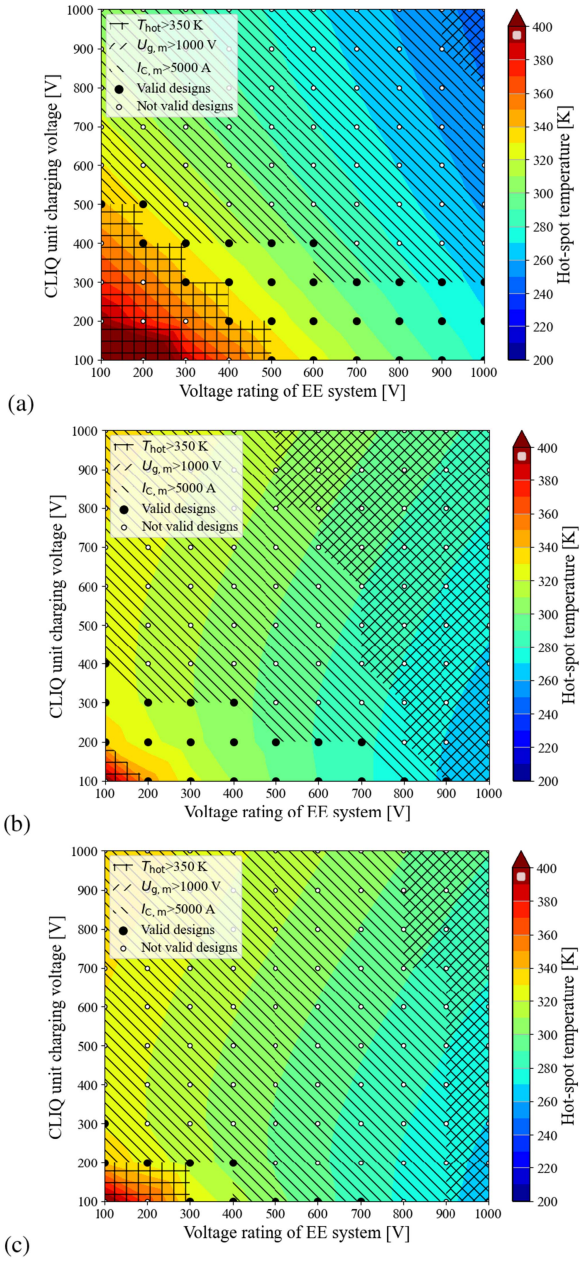

Fig. 6. Optimization of the EER+CLIQ protection system. Simulated adiabatic hot-spot temperature versus charging voltage of the CLIQ unit and rating of the EER system. The design space resulting in T_{hot}, U_{ground}, and I_C above requirements is ruled out with various patterns, which can overlap. Valid and not valid designs, i.e. designs respecting all requirements or not, are indicated with filled and empty scatter points, respectively. (a) EER+CLIQ-C1. (b) EER+CLIQ-C2. (c) EER+CLIQ-C3.

D. Energy Extraction and CLIQ

It is possible to combine an EE system and a CLIQ system to even further decrease the hot-spot temperature. If the charging polarity of the CLIQ unit is chosen as shown in Fig. 2, the EE and CLIQ work synergistically by imposing voltages with the same polarities across the coil sections. In fact, the EE imposes a negative voltage only over sections L_{A1} and L_{A2} (see Fig. 2) since L_B is effectively by-passed, while CLIQ imposes a positive voltage over section L_B. As a result, significantly lower CLIQ charging voltage is required to introduce the same dI/dt, and hence dB/dt and transient losses, in the coil sections.

A wide parametric study is performed to identify designs including both EE and CLIQ that minimize T_{hot} while satisfying the requirements $U_{g,m} \leq 1$ kV and $I_{C,m} \leq 5$ kA. For each of the three CLIQ configurations, the performance of the combination of EE rating voltage U_{EE0} [V] and CLIQ unit charging voltage that yields the lowest T_{hot} is reported in Table III.

A detailed analysis of the EER+CLIQ system performance is shown in Fig. 6, where the T_{hot} is plotted as a function of U_{EE0} and U_{C0}. The combinations resulting in any of T_{hot}, $U_{g,m}$, or $I_{C,m}$ being outside the requirements are ruled out. For EER+CLIQ-C1, there are a number of combinations that are acceptable, and the lowest T_{hot} is obtained for $U_{EE0} = 1$ kV and $U_{C0} = 300$ V. For EER+CLIQ-C2, a large number of combinations are discarded due to excessive $U_{g,m}$ and $I_{C,m}$. For EER+CLIQ-C3, only a few combinations are acceptable since $I_{C,m}$ is $\geq$5 kA in all but a few cases.

Considering the limitations of the existing test facility equipment, the recommended protection configuration is EER+CLIQ-C1 with U_{EE0}=1 kV and U_{C0}=300 V, which offers low T_{hot} obtained with a redundant system comprising both energy extraction and CLIQ and the easiest-to-implement CLIQ configuration (see Fig. 5). The limited reduction of T_{hot} offered by the varistor does not justify the procurement of this piece of equipment.

IV. Conclusion

A 13 T Nb_3Sn stress-managed asymmetric common-coil magnet including novel features is being developed at the Paul Scherrer Institute (PSI). The design and optimization of the quench protection system for a 0.8 m long demonstrator magnet is presented.

The electro-magnetic and thermal transients occurring during a quench discharge are modeled with the STEAM-LEDET software. The quench detection times are calculated in the case of quenches occurring in various conductor locations. Furthermore, the performances of combinations of different quench protection systems are analyzed. The presence of multiple layers in the common-coil design allows for great flexibility in the CLIQ (Coupling-Loss Induced Quench) lead positioning and coil electrical ordering. Both ingredients are optimized to significantly reduce the peak temperature and voltage to ground during a quench event.

It is shown that energy-extraction, a CLIQ system, or combined energy extraction and CLIQ are all viable options to protect this magnet, as they can maintain within acceptable limits the hot-spot temperature and peak voltage to ground reached in the magnet windings after a quench. The lowest peak voltage to ground can be achieved using CLIQ, while the lowest hot-spot temperature can be achieved by combining energy extraction and CLIQ.

The quench protection configuration including energy-extraction in combination with low-voltage CLIQ is recommended due to its good performance in terms of low hot-spot temperature and redundancy. These findings are valid for the considered magnet and test facility, and case-by-case studies are needed to analyze other applications.

REFERENCES

[1] D. Araujo, B. Auchmann, A. Brem, T. Michlmayr, A. Haziot, and E. Ravaioli, "Electromechanical design of Nb_3Sn 13 T. Stress-managed asymmetric common-coils (SMACC) a 2-in-1 dipole magnet," unpublished.

[2] D. Araujo et al., "Manufacturing and testing of the first Nb_3Sn subscale stress-managed common-coils 2-in-1 dipole magnet developed at the Paul Scherrer Institute," unpublished.

[3] E. Ravaioli, V. I. Datskov, C. Giloux, G. Kirby, H. H. J. ten Kate, and A. P. Verweij, "New, coupling loss induced, quench protection system for superconducting accelerator magnets," *IEEE Trans. Appl. Supercond.*, vol. 24, no. 3, Jun. 2014, Art. no. 0500905.

[4] E. Ravaioli, "CLIQ," Ph.D. dissertation, Univ. Twente, Enschede, Netherlands, 2015. Accessed: Jun. 19, 2015. [Online]. Available: http://doc.utwente.nl/96069/

[5] E. Ravaioli, B. Auchmann, M. Maciejewski, H. ten Kate, and A. Verweij, "Lumped-element dynamic electro-thermal model of a superconducting magnet," *Cryogenics*, vol. 80, pp. 346–356, 2016. [Online]. Available: http://www.sciencedirect.com/science/article/pii/S0011227516300832

[6] "STEAM website," 2024. [Online]. Available: https://cern.ch/steam

[7] E. Ravaioli, O. T. Arnegaard, A. Verweij, and M. Wozniak, "Quench transient simulation in a self-protected magnet with a 3-D finite-difference scheme," *IEEE Trans. Appl. Supercond.*, vol. 32, no. 6, Sep. 2022, Art. no. 4005205.

[8] E. Ravaioli et al., "Modeling of inter-filament coupling currents and their effect on magnet quench protection," *IEEE Trans. Appl. Supercond.*, vol. 27, no. 4, Jun. 2017, Art. no. 4000508.

[9] M. Mentink and E. Ravaioli, "Analysis of MQXFS5 CLIQ tests of November 2017," CERN, Geneva, Switzerland, Tech. Rep. EDMS 1930202, 2018.

[10] E. Ravaioli et al., "Quench protection of the first 4-m-long prototype of the HL-LHC Nb_3Sn quadrupole magnet," *IEEE Trans. Appl. Supercond.*, vol. 29, no. 5, Aug. 2019, Art. no. 4701405.

[11] M. Janitschke, M. Mentink, F. Murgia, D. Pracht, E. Ravaioli, and A. P. Verweij, "A simplified approach to simulate quench development in a superconducting magnet," *IEEE Trans. Appl. Supercond.*, vol. 31, no. 5, Aug. 2021, Art. no. 4000905.

[12] D. Mayr et al., "Simulating quench transients in the self-protected HL-LHC high order corrector magnets," *IEEE Trans. Appl. Supercond.*, vol. 34, no. 5, Aug. 2024, Art. no. 4003605.

[13] B. Caiffi et al., "Protection scheme effectiveness study for the high-luminosity LHC MBRD magnet," *IEEE Trans. Appl. Supercond.*, vol. 33, no. 5, Aug. 2023, Art. no. 4701304.

[14] H. ten Kate, H. Boschman, and L. Van de Klundert, "Longitudinal propagation velocity of the normal zone in superconducting wires," *IEEE Trans. Magn.*, vol. MAG-23, no. 2, pp. 1557–1560, Mar. 1987.

[15] B. J. Maddock and G. B. James, "Protection and stabilisation of large superconducting coils," *Proc. Inst. Elect. Engineers*, vol. 115, no. 4, pp. 543–547, Apr. 1968.

[16] J. Schultz, "Protection of superconducting magnets," *IEEE Trans. Appl. Supercond.*, vol. 12, no. 1, pp. 1390–1395, Mar. 2002.

[17] F. Sonnemann, "Resistive transition and protection of LHC superconducting cables and magnets," 2001. Accessed: Feb. 12, 2001. [Online]. Available: https://cds.cern.ch/record/499591

[18] L. Bottura, "Magnet quench 101," Jan. 2014, *arXiv:1401.3927*, Comments: 9 pages, Contribution to WAMSDO 2013: Workshop on Accelerator Magnet, Superconductor, Design and Optimization; 15–16 Jan. 2013, CERN, Geneva, Switzerland. [Online]. Available: http://cds.cern.ch/record/1643429/export/hx?ln=en

[19] F. Rodriguez Mateos et al., "Design and manufacturing of the first industrial-grade CLIQ units for the protection of superconducting magnets for the high-luminosity LHC project at CERN," *IEEE Trans. Appl. Supercond.*, vol. 28, no. 3, Apr. 2018, Art. no. 4702504.

[20] G. H. Morgan, "Theoretical behavior of twisted multicore superconducting wire in a time-varying uniform magnetic field," *J. Appl. Phys.*, vol. 41, no. 9, pp. 3673–3679, 1970. [Online]. Available: http://scitation.aip.org/content/aip/journal/jap/41/9/10.1063/1.1659491

[21] W. J. Carr, "AC loss in a twisted filamentary superconducting wire," *J. Appl. Phys.*, vol. 45, no. 2, pp. 929–938, 1974. [Online]. Available: http://scitation.aip.org/content/aip/journal/jap/45/2/10.1063/1.1663341

[22] A. P. Verweij, "Electrodynamics of superconducting cables in accelerator magnets," Ph.D. dissertation, Univ. Twente, Enschede, Netherlands, 1995. Accessed: Sep. 15, 1995. [Online]. Available: https://cds.cern.ch/record/292595

[23] E. Ravaioli et al., "Towards an optimized coupling-loss induced quench protection system (CLIQ) for quadrupole magnets," *Phys. Procedia*, vol. 67, pp. 215–220, 2015. [Online]. Available: http://www.sciencedirect.com/science/article/pii/S1875389215004186